International Biodeterioration & Biodegradation 64 (2010) 489–498

Contents lists available at ScienceDirect

International Biodeterioration & Biodegradation

journal homepage: www.elsevier.com/locate/ibiod

Influence of water hardness on concrete surface deterioration caused by nitrifying biofilms in wastewater treatment plants

Andreas Leemann [a,*], Barbara Lothenbach [a], Hansruedi Siegrist [b], Cathleen Hoffmann [a]

[a] Empa, Überlandstr. 129, 8600 Dübendorf, Switzerland
[b] EAWAG, Überlandstr. 133, 8600 Dübendorf, Switzerland

ARTICLE INFO

Article history:
Received 3 December 2009
Received in revised form
25 March 2010
Accepted 25 March 2010
Available online 12 June 2010

Keywords:
Biodeterioration
Nitrification
Acid attack
Concrete
Erosion

ABSTRACT

In aeration tanks of wastewater treatment plants (WWTP), biodeterioration can lead to a partial dissolution and ensuing erosion of the concrete due to an acid attack caused by the nitrifying biofilm covering the tank surface. In this study, concrete samples were exposed in four different WWTP. The CaO content of the cement used, the water-to-cement ratio, and curing affect the resistance of the concrete to acid attack. However, both experimental data and thermodynamic modeling show that water hardness is the dominating parameter for surface erosion. In the presence of high water hardness, the protons produced by the nitrifiers are buffered and the calcite precipitation occurring in all concrete samples is increased. This results in a decrease of porosity near the surface and higher mass transfer resistance against carbon dioxide and therefore in lower deterioration rates of the concrete.

1. Introduction

Biodeterioration of inorganic building materials is a widespread phenomenon (e.g., Parker, 1945; Sand and Bock, 1991; Jozsa et al., 1996; Sand, 1997; Okabe et al., 1999; Warscheid and Braams, 2000). One area of concern is concrete structures used to transport and treat wastewater. The most severe attack is usually observed in sewer pipes. Sulfur present in the wastewater is reduced by sulfur reducing bacteria to hydrogen sulfide gas that diffuses to the water-free soffit of the sewer, where it is in turn oxidized by thiobacilii to sulfuric acid (e.g., Parker, 1945; Davis et al., 1998; Nica et al., 2000; Vincke et al., 2001). This leads to a combined acid and sulfate attack on the concrete. However, concrete deterioration can also occur in the nitrifying basins of wastewater treatment plants (WWTP). In such aerated tanks, ammonium is oxidized in two steps (Eqs. (1) and (2)) to nitrate. In the first step, ammonia is oxidized by ammonia oxidizer to nitrite; the nitrite is then oxidized by nitrite oxidizer to nitrate:

$$NH_3 + 1.5\ O_2 \rightarrow NO_2^- + H_2O + H^+ \quad (1)$$

$$NO_2^- + 0.5\ O_2 \rightarrow NO_3^- \quad (2)$$

$$NH_3 + 2.0\ O_2 \rightarrow NO_3^- + H_2O + H^+ \quad (1+2)$$

The autotrophic nitrifying bacteria belong to *Nitrosomonas*, *Nitrobacter*, *Nitrospira*, and *Nitrosococcus* species (e.g., Juretschko et al., 1998; Aoi et al., 2000; Dionisi et al., 2002; You and Chen, 2008; Kocamemi and Çeçen, 2009; Gujer, 2010). The protons produced by the ammonium oxidizer are buffered by the natural bicarbonate buffer of the wastewater (Eq. (3)) and 1 mol of bicarbonate is consumed per mole of free ammonia nitrified:

$$H^+ + HCO_3^- = CO_2 + H_2O \quad (3)$$

$$NH_3 + 2.0\ O_2 + HCO_3^- \rightarrow NO_3^- + 2\ H_2O + CO_2 \quad (1+2+3)$$

During heterotrophic denitrification 1 mol of bicarbonate is again produced per mole of nitrate reduced to molecular nitrogen:

$$NO_3^- + \text{organic carbon} \rightarrow HCO_3^- + 0.5\ N_2 + xCO_2 + yH_2O \quad (4)$$

Depending on the bicarbonate concentration of the water, on the fraction of nitrate denitrified, and on the efficiency of the CO_2

* Corresponding author. Tel.: +41 44 823 44 89; fax: +41 44 823 40 35.
E-mail addresses: andreas.leemann@empa.ch (A. Leemann), barbara.lothenbach@empa.ch (B. Lothenbach), hansruedi.siegrist@eawag.ch (H. Siegrist), cathleen.hoffmann@empa.ch (C. Hoffmann).

0964-8305/$ – see front matter © 2010 Elsevier Ltd. All rights reserved.
doi:10.1016/j.ibiod.2010.03.009

Table 1
Composition of the cements (LOI = loss on ignition/n.a. = not analyzed).

Type	CaO [%]	SiO_2 [%]	Al_2O_3 [%]	Fe_2O_3 [%]	MgO [%]	K_2O [%]	Na_2O [%]	SO_3 [%]	CO_2 [%]	LOI [%]	Density [kg m^{-3}]
CEM I 42.5 N	62.6	19.5	4.6	2.8	1.9	0.95	0.15	3.1	1.5	2.8	3.14
CEM II/A-LL 42.5 N	61.1	17.2	4.1	2.5	1.7	0.86	0.11	2.8	5.7	7.6	3.07
CEM III/B 32.5 N	48.5	30.5	9.7	1.9	4.5	0.61	0.29	2.9	0.6	n.a	2.93

stripping of the aeration (modern fine bubble aeration systems have a high oxygen yield to reduce energy consumption and consequently a low CO_2 stripping efficiency), the pH in the nitrification tanks remains in the range of 6.6–7.5. However, a lower pH is established at the concrete surface due to the acid production and the mass transfer effects in the nitrifying biofilm covering the concrete (Siegrist and Gujer, 1987). This induced acid attack causes a partial dissolution and a weakening of the cement paste leading to the erosion of the concrete surface. As a result, the thickness of the concrete cover protecting the reinforcement may be decreased and with it the durability of the structure. The degree of deterioration is influenced by the concrete composition (Leemann et al., 2009, 2010). Deteriorated concrete shows a characteristic microstructure at the surface, with leached paste, but also the formation of a dense calcite layer close to the surface (Leemann et al., 2009, 2010). This layer is formed due to the reaction between the calcium oxide of the concrete and the CO_2 penetrating from the nitrifying biofilm into the concrete. The leached porous silica gel layer at the surface and the calcite layer (Fig. 2) decrease diffusivity and act as a buffer for the attacking carbon dioxide, thereby increasing concrete resistance. However, the influence of water hardness, the progress of the biologically induced deterioration with time, and the resulting rate of surface erosion are not known.

In this study, the reasons for the variability of concrete erosion in different wastewater treatment plants and the erosion kinetics were investigated. Concrete specimens of different composition were exposed in the nitrification basins of four different WWTPs. The water hardness in the four different plants varied between 19.5 and 30.0 °fH, corresponding to 4–6.4 mM of dissolved bicarbonate. After exposure, microstructure and chemical composition of the specimens exposed in one WWTP were analyzed. Additionally, thermodynamic modeling was used to further investigate the effect of bicarbonates on the dissolution of hydrates and on calcite precipitation.

2. Materials and methods

2.1. Concrete mixtures

Three concrete mixtures were produced with a water-to-cement ratio (w/c) of 0.50 and a cement content of 325 kg m^{-3} using the following cement types: CEM I (5% limestone filler), CEM II/A-LL (up to 20% limestone filler), and CEM III/B (up to 80% slag; Tables 1 and 2). In a second mixture with CEM I, a w/c of 0.40 and a cement content of 375 kg m^{-3} were used. Concrete cubes with a side length of 150 mm were produced and de-molded after 24 h. One set of cubes was stored at a temperature of 20 °C and a relative humidity of 70% for 28 days to simulate "bad" curing. The other set was cured in tap water at 20 °C for 90 days to simulate "good" curing and optimize cement hydration.

2.2. Properties of hydrated samples

Compressive strength was measured on three cubes at the age of 28 days ("bad" curing) and 90 days ("good" curing) according to European standard EN 12504-1.

Oxygen diffusion (Lawrence, 1984; Buenfeld and Okundi, 1998) was determined on two cores (diameter of 100 mm, length of 50 mm) taken from surface part of cubes stored for 28 days ("bad" curing) and 90 days ("good" curing). Before measuring oxygen diffusivity, the cores were first kept at 20 °C and 35% relative humidity for seven days and then dried in an oven at 50 °C for another seven days. On one side of the cores, an oxygen flow was applied and on the other side, a nitrogen flow was applied; the two had identical pressures. The oxygen content in the nitrogen flow was measured until equilibrium was reached. Afterwards, the oxygen diffusion coefficient was calculated according to Lawrence (1984).

2.3. Characteristics of the different WWTPs

Modern wastewater treatment plants include in their biological treatment organic carbon removal, full nitrification, and partial denitrification. For example, at the river Rhine catchment 70–80% nitrogen removal is requested. Nitrate is denitrified with the degradable organic carbon of the wastewater by recycling nitrate-containing water and sludge from the aerated nitrifying zone to the non-aerated denitrifying zone upstream (pre-denitrification) or by changing between aerobic (nitrifying) and mixing (denitrifying) conditions (i.e., intermittent denitrification). The main applied systems are the activated sludge system working with suspended biomass, and the biofiltration containing system with fixed biomass (biofilm system). In the activated sludge system, the suspended solids have to be continuously separated from the treated wastewater by sedimentation or membrane separation and transported to the inlet of the bioreactor where they are again mixed with untreated wastewater. In biofiltration, the wastewater is treated by passing through a filter system with a fixed biomass. Denitrification is always upstream of nitrification.

The concrete erosion in three nitrifying/denitrifying activated sludge systems (WWTPs 19, 26, and 30) and one biofiltration system (WWTP 24) were investigated (Table 3). In biofiltration, the air flow per cubic meter of treated wastewater is significantly higher than in the activated sludge system due to the lower height of the filter compared to the activated sludge tank. Moreover, the lower oxygen input efficiency results in a much higher carbon dioxide stripping and therefore a significantly higher pH in WWTP 24 (Table 3).

2.4. Exposure in different WWTPs

At the age of 28 days ("bad" curing) and 90 days ("good" curing), respectively, the concrete prisms were exposed in four different WWTPs.

Table 2
Concrete mix design.

Concrete	C-OPC-1	C-LS	C-SL	C-OPC-2
Cement	CEM I 42.5 N	CEM II/A-LL 42.5 N	CEM III/B 32.5 R	CEM I 42.5 N
Cement content [kg m^{-3}]	325	325	325	375
Aggregate 0/32 mm [kg m^{-3}]	1940	1935	1920	1940
Water [kg m^{-3}]	163	163	163	163
Superplasticizer [kg m^{-3}]	–	–	–	5.7
w/c	0.50	0.50	0.50	0.40

Table 3
Information about the biological treatment of the WWTPs, location of the prisms and water hardness. French water hardness: 10 °fH = 1 mmol carbonate l^{-1}.

WWTP	Biological treatment system with nitrification and partial denitrification	Alkalinity drinking water [°fH]	Average alkalinity tank[a]	Mean pH_{tank} (measured/ estimated)	O_2 concentration in tank [mg l^{-1}]	Location of prisms
WWTP-19	Activated sludge with intermittent denitrification	19.5 ± 2.5	19 °fH = 3.8 mM	6.6	1	Nitrification tank (~1.5 m above floor)
WWTP-24	Biofiltration with nitrification and pre-denitrification	24.5 ± 6	24 °fH = 4.8 mM	7.4	5	1 m deep in the aerated filter-bed
WWTP-26	Activated sludge with pre-denitrification	26.5 ± 3.5	26 °fH = 5.2 mM	6.9	2	Nitrification tank (~1.5 m above floor)
WWTP-30	Activated sludge system with pre-denitrification	30 ± 12	30 °fH = 6.0 mM	7.0	2	Nitrification tank (~1.5 m above floor)

[a] Average alkalinity in aeration tank = average alkalinity − $C_{NO_3-N,out}$/14 (Nitrification consumes 1 mM alkalinity per 14 g NH_3–N nitrified and denitrification produces 1 mM alkalinity per 14 g NO_3–N denitrified, 1 °fH = 0.2 mmol l^{-1} = 0.2 mM).

Prisms with a size of 72 × 72 × 150 mm^3 were cut from the cubes of the four different concrete mixtures ("bad" and "good" curing). Each prism had two cut surfaces and two uncut surfaces along its longitudinal axis. The cut surfaces were used to assess the effect of large aggregates that are not present on uncut surfaces. Both ends of the prisms were coated with epoxy resin, resulting in two layers with a width of 20 mm. For measuring the position of the surface, the prisms were positioned on the base plate of a stand provided with a depth gauge. The tip of the gauge was a cylinder with a diameter of 1.5 mm. A steel plate with angles on three sides and 20 small holes was placed on top of the prism (Fig. 1), ensuring identical positioning. The repeatability of the method (single measurement) as tested is around 0.02 mm.

The position of the surface was measured before the exposure and after 94, 191, and 282 days of exposure. The measured sides (one cut and one uncut surface) were cleaned with a brush before measuring. The erosion was calculated by subtracting the measured surface position from the original surface position.

After an exposure of 282 days, the prisms of WWTP-27 were removed and used to analyze microstructure and chemical composition of the surface layers.

2.5. Microstructural analysis

From the midsection of the samples exposed in WWTP-27, a slice (thickness of 1.5 cm) was cut perpendicular to the length axis, dried in an oven at 50 °C for three days, impregnated with epoxy resin, and polished. The analysis of the surface layers was conducted with an environmental scanning electron microscope (ESEM-FEG XL30). The carbon-coated samples were studied in the high-vacuum mode (2.0–6.0 10^{-6} Torr) with an accelerating voltage of 15 kV and a beam current of 275–280 μA. The chemical composition of the surface layers of C-OPC-2 was determined with energy dispersive X-ray spectroscopy (EDX). An EDAX 194 UTW detector, a Philips digital controller, and Genesis Spectrum Software (Version 4.6.1) with ZAF corrections were used. In each layer, 10 area scans (~20 × ~20 μm) of the hydration products were made to analyze their chemical composition.

Fig. 1. Measurements on prism with coated ends using a steel plate with 20 holes on a stand with calibrated depth gauge.

The software for segmentation of the phases was developed in Matlab. Layers of different porosity were defined. Porosity was defined by an upper threshold value of 80 in the grey scale of 0–255. The pixel size of the images used for the analysis was 0.93 μm. The porosity was analyzed in bands with a width of 0.93 μm as a function of depth.

2.6. Thermodynamic modeling

Thermodynamic modeling was used to study the chemical changes associated with the ingress of carbonate-free and carbonate-containing solutions in OPC. Thermodynamic modeling can be used to calculate the changes associated with the ingress of carbon dioxide or acid in a concrete sample. The ingress of carbon dioxide can be mimicked in these calculations assuming that the core of the sample is in contact with no additional solution containing carbon dioxide, while the area near the surface is in contact with large quantities of solution. Even though these calculations do not relate directly to time and space, they represent a convenient way to calculate the different conditions that a concrete sample submerged in carbonate solutions experiences. Such a modeling approach has the advantage that the calculations are very fast and flexible as no transport equations have to be considered. However, the calculated data relate neither to time nor to distance from the surface.

Thermodynamic modeling was carried out using the Gibbs free energy minimization program GEMS (Kulik, 2007). The GEMS program is a broad-purpose geochemical modeling code that computes equilibrium phase assemblage and speciation in a complex chemical system from its total bulk elemental composition. Chemical interactions involving solids, solid solutions, and aqueous electrolytes are considered simultaneously. The speciation of the dissolved species as well as the kind and amount of solids precipitated are calculated. The thermodynamic data for aqueous species as well as for many solids were taken from the PSI–GEMS thermodynamic database (Hummel et al., 2002; Thoenen and Kulik, 2003). Solubility products for cement minerals including ettringite, different AFm phases, hydrogarnet, calcium–silicon–hydrate (C–S–H), and hydrotalcite were taken from the

recent cemdata07 compilation (Lothenbach et al., 2008). For C–S–H an ideal solid solution between a jennite and a tobermorite type C–S–H was considered, but no solid solution between tobermorite and amorphous SiO_2. For the calculations it was assumed that all of the Portland cement had reacted. In the calculations the dissolution of amorphous SiO_2 gel was prevented by lowering its solubility products by 2.5 log units, as the SiO_2 dissolution kinetics is very slow at neutral and slightly alkaline pH conditions (Dove, 1994; Bickmore et al., 2006).

The most important minerals formed during cement hydration are listed in Table 4. To calculate the dissolution of the hydrate assemblages, the presence of 3.2 mmol l^{-1} and the complete absence of carbonate were taken into account, corresponding to the 32 (WWTP-32) and 0 °fH. The later value for water hardness does not correspond to the conditions in a WWTP but was chosen to show the effect of carbonate-free solutions. The carbonate was assumed to be present as 1.07 mmol l^{-1} $CaCO_3$ and 2.13 mmol l^{-1} H_2CO_3, to be consistent with a pH value of 7. For porosity and pH calculations, intermediate steps of 8 and 16 °fH were added.

3. Results

3.1. Concrete properties

The compressive strength of the concrete mixtures with "good" curing is higher and O_2-diffusion coefficients are lower due to a higher degree of hydration (Table 5). C-SL shows the biggest difference between "good" and "bad" curing as it hydrates relatively slowly and is affected the most by the differences in curing.

3.2. Situation at the water–biofilm–concrete interface

Due to the nitrifying activity (Eqs. (1)–(3)) in the biofilm oxygen, bicarbonate and ammonia have to be transported into the biofilm by molecular diffusion, and nitrate, together with carbon dioxide, has to be transported out of the film. The mass transfer resistance of the laminar layer and the biofilm cause a decreasing concentration profile for oxygen, ammonia, and bicarbonate and an increasing profile for nitrate and carbon dioxide, resulting in a decreasing pH in the biofilm (Fig. 2). A small fraction of the CO_2 produced by the nitrifying biofilm penetrates into the concrete, where it continuously dissolves the calcite layer at the outside ($CaCO_3 + CO_2 \rightarrow Ca^{2+} + 2HCO_3^-$) and forms it at the inside ($Ca^{2+} + 2OH^- + CO_2 \rightarrow CaCO_3$).

Due to higher stripping efficiency of the carbon dioxide in the biofilter of WWTP 24 than in the activated sludge systems (see Section 2.3), the carbon dioxide concentration is significantly lower and therefore the pH in the bulk liquid of the biofilter significantly higher at the same water hardness. However, the carbon dioxide increase within the biofilm of the biofilter and therefore the pH drop are higher, because the oxygen concentration and therefore the nitrification activity are higher. As a result, the pH inside the biofilm of the biofilter is only slightly higher compared to the one in the activated sludge tank. Water hardness is therefore a better indicator to estimate concrete erosion in WWTPs than the bulk pH or the type of the wastewater treatment system (compare Figs. 14 and 15).

Table 4
Hydrates and their composition.

Hydrates	Composition
Jennite[a]	$1.7CaO \cdot SiO_2 \cdot 4H_2O$
Tobermorite[a]	$0.8CaO \cdot SiO_2 \cdot 1.3H_2O$
Ettringite	$3CaO \cdot Al_2O_3 \cdot 3CaSO_4 \cdot 32H_2O$
Monocarbonate	$3CaO \cdot Al_2O_3 \cdot CaCO_3 \cdot 11H_2O$
Monosulfate	$3CaO \cdot Al_2O_3 \cdot CaSO_4 \cdot 12H_2O$
Portlandite	$Ca(OH)_2$
Hydrotalcite	$Mg_4 \cdot Al_2(OH)_{14} \cdot 3H_2O$

[a] In cements ill-crystalline jennite or tobermorite-like phases are present, which are denoted as "C–S–H": calcium silicate hydrate of variable composition.

Table 5
Compressive strength and oxygen diffusion coefficients of the four concrete mixtures.

Properties	Age, curing	C-OPC-1	C-LS	C-SL	C-OPC-2
Compressive strength [MPa]	28 days, "bad"	46.5	43.7	39.9	60.6
	90 days, "good"	55.3	51.6	59.2	71.7
O_2-diffusion coefficient [10^{-8} m^2 s^{-1}]	28 days, "bad"	1.20	1.92	0.73	0.70
	90 days, "good"	0.52	0.88	0.13	0.32

3.3. Concrete deterioration in WWTP

After an exposure of 282 days, the concrete surfaces are eroded only fractions of a millimeter (Fig. 3). During this period the progress of erosion is approximately linear. The different concrete mixtures exhibit different degrees of deterioration. Concrete C-SL shows the highest erosion and C-LS the lowest. The highest individual erosion of 0.20 mm is reached by concrete C-SL with "bad" curing in WWTP-20.

The degree of deterioration is higher on the uncut surface compared to the cut surfaces (Fig. 4). The erosion on the uncut surfaces of the samples with "good" curing is about 30% lower than on the ones with "bad" curing (Fig. 5), while erosion on the cut surfaces does not differ.

The differences in erosion rate between the different WWTP are substantial (Fig. 6). The mean values of the uncut surfaces for all WWTP are about four times higher for WWTP-20 than for WWTP-32.

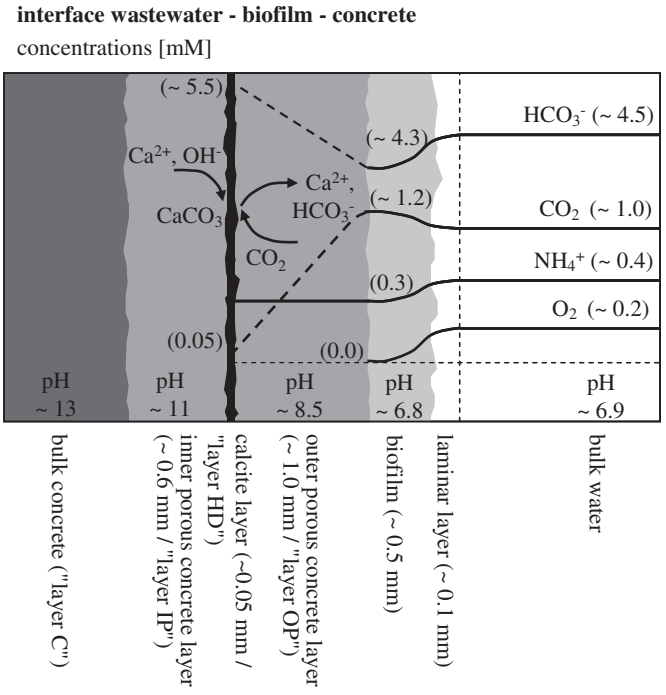

Fig. 2. Situation at the interface of wastewater-biofilm-concrete. Thickness of the layers in the concrete after two years of exposure in a WWTP plant according to Leemann et al. (2010).

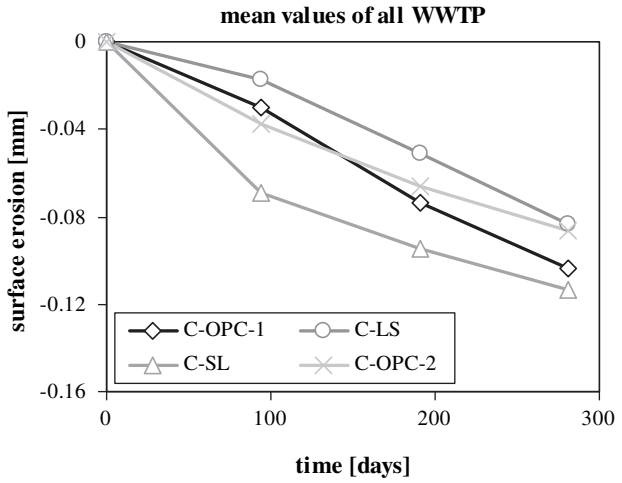

Fig. 3. Surface erosion of the uncut sides of the different concrete mixtures ("bad" and "good" curing). Mean values for all WWTP.

3.4. Characteristics of concrete surfaces in WWTPs

The concrete surface of all mixtures shows the same characteristics with three altered layers. As the grey scale values in the backscattering electron mode indicate the porosity of the material, these layers can be distinguished both visually (Figs. 7 and 8) and quantitatively (Fig. 9):

layer OP: outer porous layer
layer HD: highly dense layer
layer IP: inner porous layer
layer C: unaltered concrete

The cement paste of the unaltered concrete in layer C shows a porosity of 10%, while an increase to about 25% is present in layer IP. In the narrow layer HD, the values decrease sharply to 10% and lower before they increase again in the layer OP up to about 55%. In the example image used (Fig. 7), this layer (and with it the original concrete surface) is not preserved entirely, as some material was eroded either in the WWTP or during sample preparation. As a result, the surface seen in Fig. 7 does not entirely correspond to the original concrete surface.

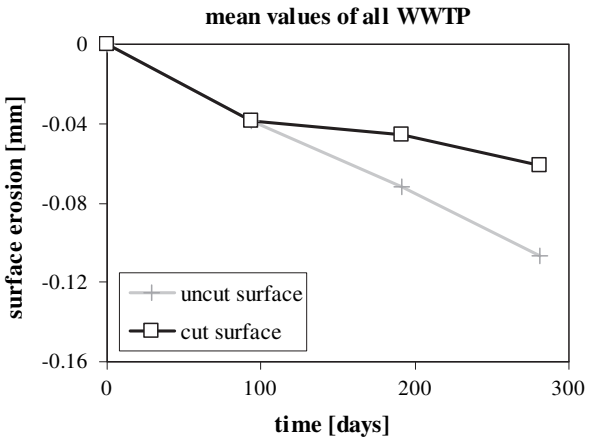

Fig. 4. Surface erosion of the cut and uncut surfaces ("bad" and "good" curing). Mean values for all concrete mixtures and WWTP.

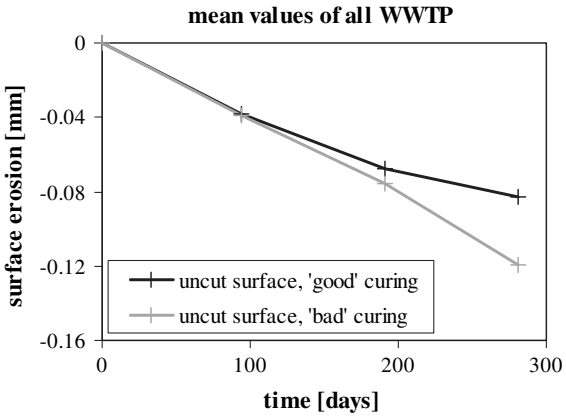

Fig. 5. Surface erosion of the uncut surfaces. Mean values for all concrete mixtures and WWTP.

The analysis of the chemical composition of these layers in concrete C-OPC-2 shows that layer IP is depleted in Ca, layer HD is enriched in Ca, and layer OP is again depleted in Ca compared to the unaffected concrete. As Si has a low solubility, these differences are best shown as the changes in Ca/Si-ratio (Fig. 10). Additionally, the S/Si ratio decreases toward the surface of the concrete, while the Al/Si and Fe/Si-ratio both increase (Fig. 11).

3.5. Thermodynamic modeling

Thermodynamic modeling was used to calculate the changes associated in the different concretes with the presence of solutions having a water hardness of 0, 8, 16, or 32 °fH and a pH of 7. In the calculations, only the interaction of the solution with the cement paste was considered, while a complete cement hydration and no interaction with the aggregate was assumed.

The unaffected core of concrete C-OPC is calculated to consist mainly of C–S–H, portlandite, ettringite, and monocarbonate, with smaller quantities of calcite and hydrotalcite (Fig. 12A). Upon the ingress of the 3.2 mM carbonate solution, the calculations predict that first portlandite becomes unstable and then the Ca/Si-ratio of the C–S–H starts to decrease (Fig. 12A). Eventually also the monocarbonate and ettringite become unstable, forming calcite and small quantities of strätlingite ($Ca_2Al_2SiO_2(OH)_{10}\cdot 3H_2O$). This leads to an inner zone that is leached with respect to calcium and sulfate. Nearer to the surface also the remaining C–S–H is leached to form

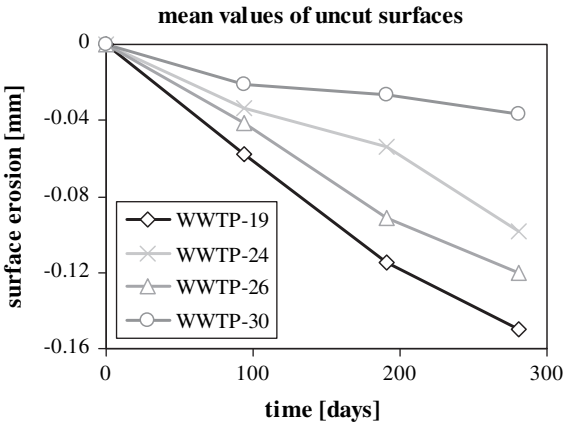

Fig. 6. Surface erosion of the uncut surfaces in the different WWTP. Mean values for all concrete mixtures.

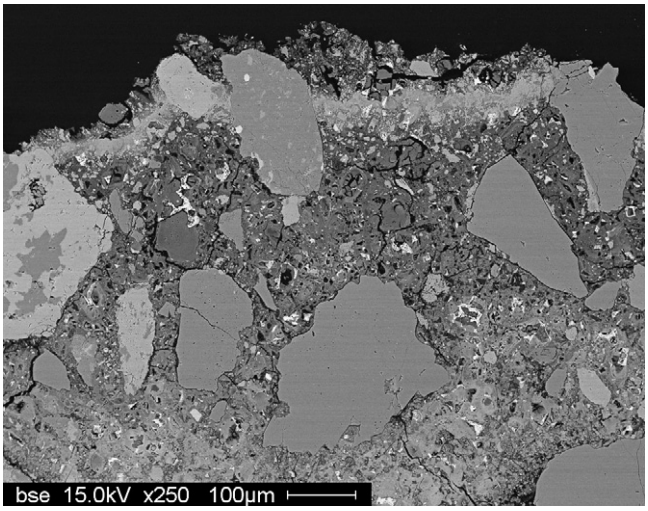

Figs. 7. Surface of concrete C-OPC-2 exposed in WWTP-26. The different layers are identified by their porosity indicated by the grey scale values of the paste: porous areas are dark, dense areas are bright.

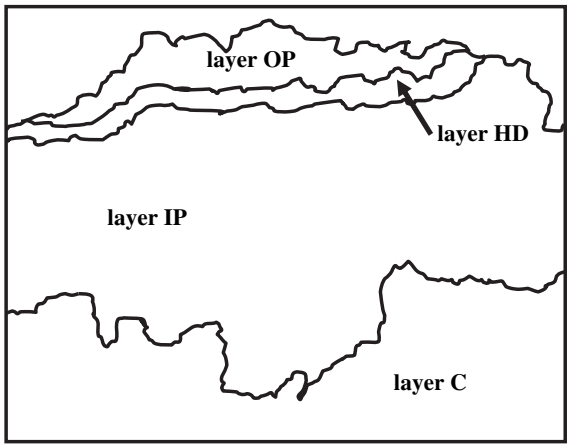

Fig. 8. Surface of concrete C-OPC-2 exposed in WWTP-26. The different layers are identified by their porosity indicated by the grey scale values of the paste: porous areas are dark, dense areas are bright.

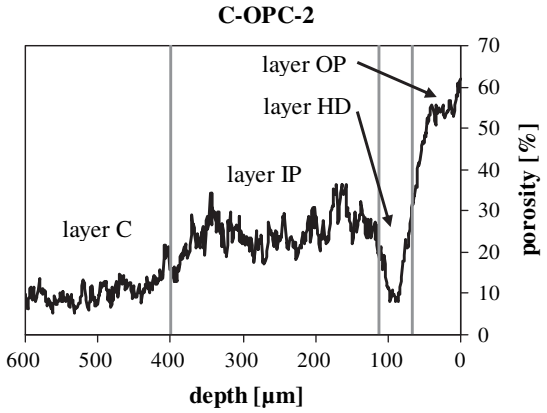

Fig. 9. Porosity distribution of the paste (not including aggregates > 20 µm) at the surface of concrete C-OPC-2 as analyzed from Fig. 7 (WWTP-26).

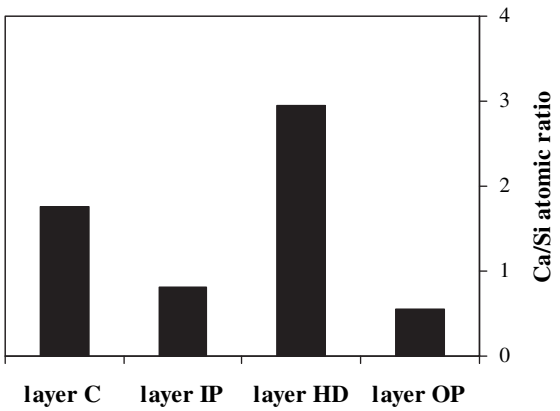

Fig. 10. Atomic ratio of Ca/Si in the different layers of concrete C-OPC-2 (WWTP-26).

calcite and amorphous silica gel. The carbon dioxide of the penetrating solution reacts with the dissolved calcium ions and leads to the formation of a calcite layer in a zone with a calculated pH in the range of 7–11.5. Additional calcium to form calcite is also leached from monocarbonate, ettringite, and the C–S–H phase (Fig. 12A). The layer that is formed fills up a significant portion of the available pore space. While the calcite layer is stable within the cement paste, at the surface calcite is unstable relative to the surrounding solution; however, amorphous SiO_2, $Al(OH)_3$ and $Fe(OH)_3$ gel will persist at the surface. Note that the dissolution of amorphous SiO_2 gel was suppressed in the thermodynamic calculations, as its dissolution kinetics are very slow at near neutral pH conditions. The calculated sequence of different layers agrees with the experimental observations in this study (see Figs. 7–11). The formation of a calcite layer near the surface results in a densification of the cement paste near the surface and thus in reduced porosity (Fig. 13A).

A reduced amount of carbonates in the solution is calculated to result in a decrease of the amount of calcite formed and thus in a higher porosity near the surface (Fig. 13A). In the absence of carbonate in the interacting solution (Fig. 12B), no calcite layer is calculated to form. The surface layer of the samples will only be leached, resulting in a low degree of space filling (Fig. 13A). The presence or absence of carbonate not only influences the formation of calcite and the calculated porosity, but also changes the pH of the solution. In the absence of carbonate, a pH of 11 or higher is predicted throughout the sample due to the leaching of the alkalis from the hydrated cement (Fig. 13B). The carbonate-containing

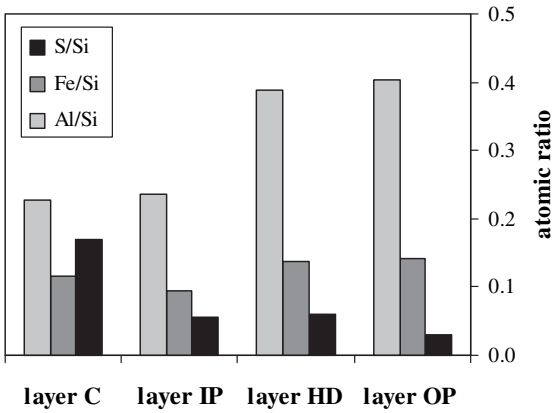

Fig. 11. Atomic ratio of S/Si, Fe/Si and Al/Si in the different layers of concrete C-OPC-2 (WWTP-26).

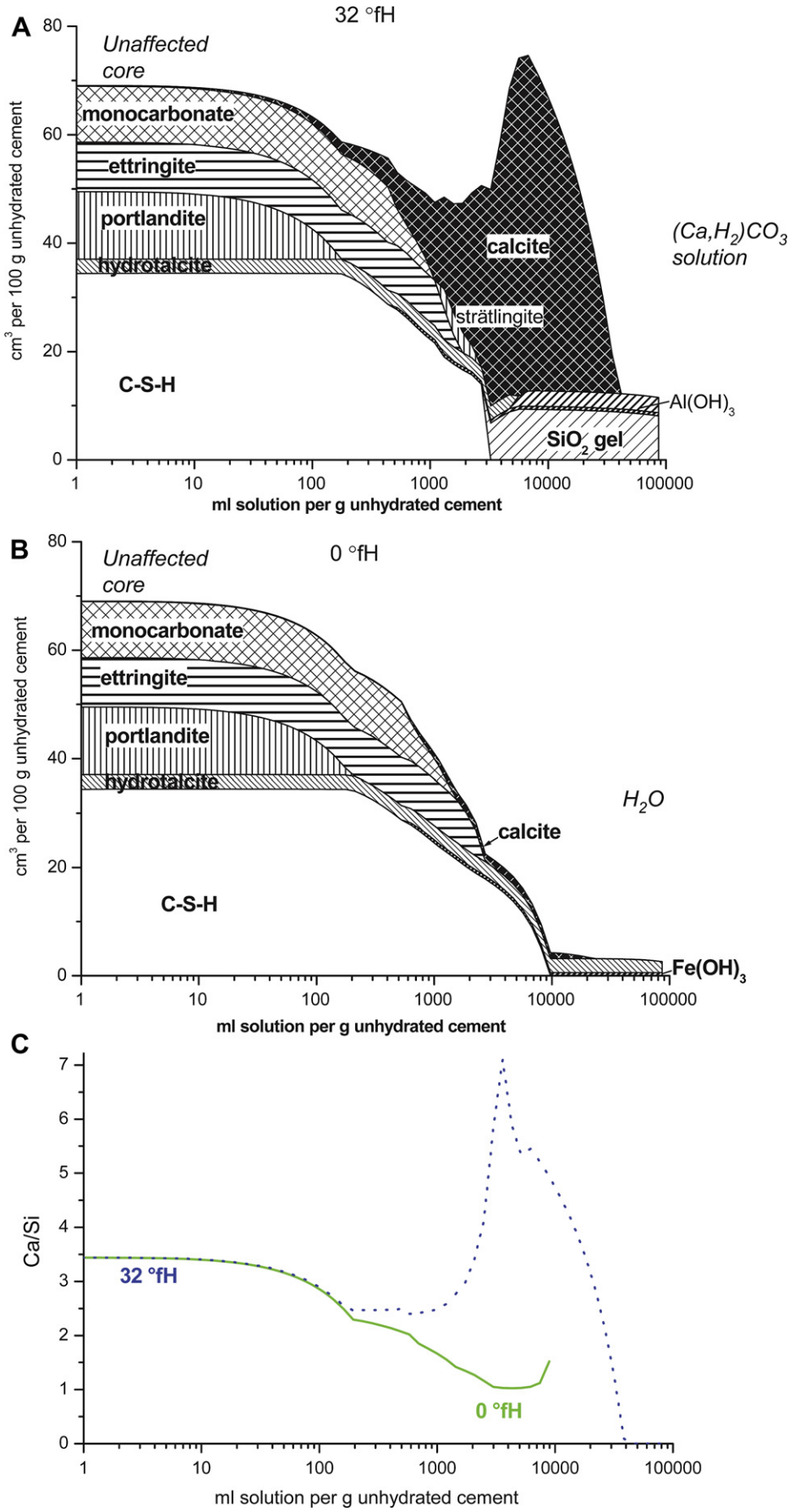

Fig. 12. Calculated changes in the hydrate assemblage of C-OPC upon the ingression of a solution containing A) 3.2 mM carbonate (32 °fH) or B) no carbonate (0 °fH). A complete reaction of the Portland cement clinker was assumed. C) Calculated Ca/Si-ratio of the cement paste. A complete reaction of the Portland cement clinker was assumed.

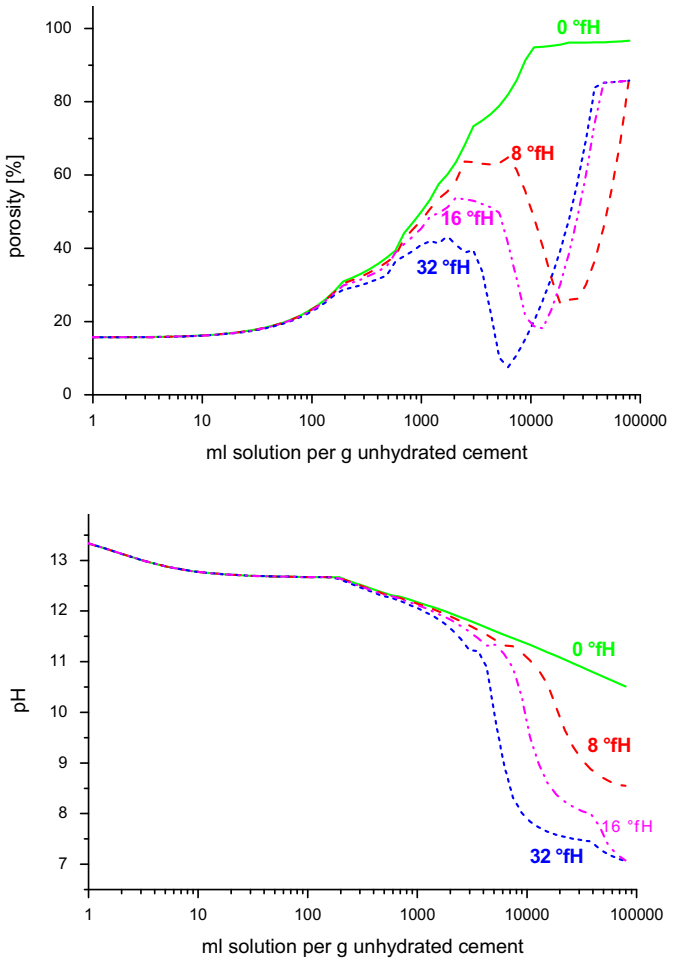

Fig. 13. Calculated changes of A) capillary porosity and B) pH of C-OPC upon the ingression of a solution containing 3.2, 1.6, 0.8 mM of carbonate (32, 16, 8 °fH) or no carbonate (0 °fH). A complete reaction of the Portland cement clinker was assumed.

sample is much more buffered, leading to a strong decrease of pH near the surface of the sample. This strong decrease of pH is calculated to somewhat stabilize SiO_2 gel and to destabilize hydrotalcite, resulting in the formation of amorphous $Al(OH)_3$ gel near the surface. The presence of such a SiO_2 and $Al(OH)_3$ gel in the presence of carbonate-containing solutions is consistent with the chemical analysis of the microstructure.

4. Discussion

The porosity and composition of the surface layers of the concrete samples exposed in the different WWTPs show the same general trends as in the concretes already described in detail in Leemann et al. (2010). Portlandite is dissolved and C–S–H is decalcified by the acid attack, leading to the observed calcium depletion in the layers IP and OP. The low porosity and high calcium content in layer HD are the result of the calcite precipitation caused by the reaction between dissolved calcium and the carbon dioxide present in the attacking solution. The hydrates containing sulfur have a relatively high solubility and therefore sulfur content in the solid decreases toward the surface. The opposite applies to Al and Fe, which both have a low solubility. The results of thermodynamic modeling confirm the experimental results and clearly explain the formation of a calcite layer near the surface in the presence of carbonate-containing solutions. These findings agree also with the experimentally observed formation of a dense calcite layer in oil-well cements exposed to solutions containing calcium and carbonates (Duguid et al., 2007; Neuville et al., 2008). The formation of such a calcite layer near the surface results in a densification of the binder near the surface and thus in reduced porosity (Fig. 13A).

The porosity in the different layers determined with image analysis (Fig. 9) and calculated with thermodynamic modeling (Fig. 13A) show the same relative differences but some deviations in the absolute values. Due to the resolution of the backscattering images, only larger pores (diameter > 2 μm) and porous patches in the paste are identified as "pores." Such an analysis shows differences in the pore volume determined, for example, with mercury intrusion (Münch and Holzer, 2008). On the other hand, porosity in the thermodynamic modeling is calculated indirectly by the volume of the hydrates and precipitation products and thus includes even very small pores not resolved by image analysis.

A number of different factors have been found to affect the surface erosion rate, including the type of cement, w/c, curing, and the water hardness of the WWTP.

The surface erosion of the concrete with a w/c of 0.50 has been observed to depend on the CaO contents of the cements used (Leemann et al., 2009, 2010). As CEM III/B has the lowest CaO content, the surface erosion of C-SL is the highest (Fig. 3). The opposite applies to CEM II/A-LL and with it to concrete C-LS.

The reduction of the w/c from 0.50 to 0.40 leads to a decrease of surface erosion. This is most likely due to the lower porosity in the w/c 0.4 sample and to the higher density of the cement paste in the concrete and the resulting higher CaO content per volume.

The lower surface erosion on the cut surfaces (Fig. 4) can be attributed to the effect of the coarse aggregates (diameter > 4 mm) on such surfaces. In the used mix design, aggregates contribute to about 72% of the concrete's volume fraction. As some of the large aggregates consist of silicates, they are not vulnerable to acid attack, resulting in lower surface erosion on the cut surfaces. Such aggregates can only be spalled, when the major part of cement paste around them is dissolved.

The lower surface erosion of the samples with "good" curing (uncut surfaces) is related to a better hydration at the concrete surface and a subsequent lower porosity and permeability (Table 5, Fig. 5). As curing mainly affects the surface of the concrete, smaller differences in erosion rate can be expected when the deterioration progresses further into the concrete. This is confirmed by the identical surface erosion of the cut surfaces with "good" and "bad" curing. It has to be pointed out as well that the chosen differences in curing are extreme and the effect of the curing regime can be expected to be smaller in concrete of real structures.

The degree of erosion decreases with increasing water hardness (Fig. 14). A dependence of the erosion on the bulk pH is not clearly seen (Fig. 15) because the pH in the bulk liquid depends strongly on the stripping efficiency of the aeration system (much higher for biofiltration of WWTP 24 than activated sludge systems of the other WWTPs) and less on the hardness of the wastewater (see Sections 2.3 and 3.2). Because the high water hardness acts as a buffer, dissolution of the concrete is slowed down. Additionally, thermodynamic calculations indicate that the higher the water hardness, the more calcite can precipitate just below the surface of the concrete (Fig. 12) and the lower is the porosity (Fig. 13). The formation of a dense layer results in a better protection of the concrete against further leaching and degradation. The density of the protecting calcite layer is thus not only a function of the CaO content of the cement but also of the carbonate content of the attacking solution. Also, the formation of the surface layers increases the distance from the biofilm to the

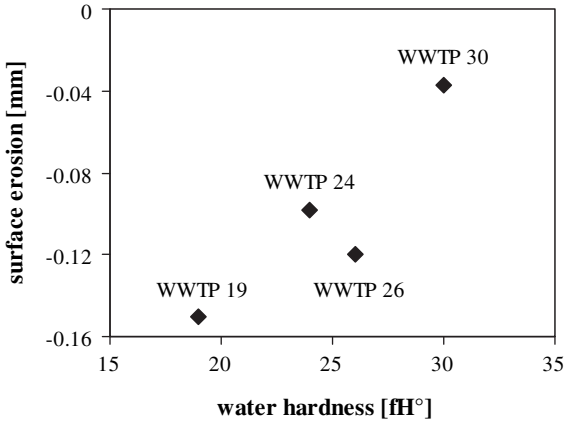

Fig. 14. Surface erosion as a function of water hardness in the aerated tanks.

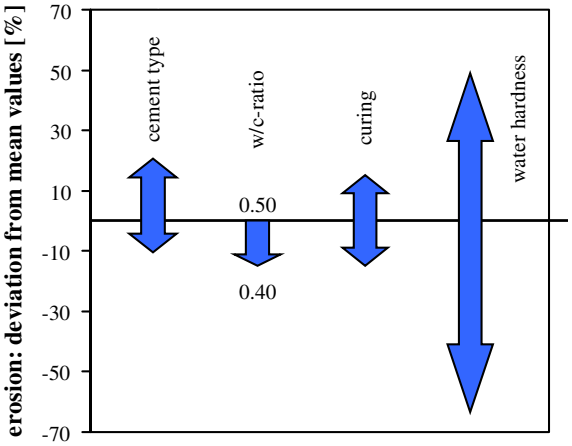

Fig. 16. Influence of different parameters on surface erosion.

unaltered concrete, reducing the acid transport and the dissolution of hydrates. A removal of these layers by cleaning of the concrete surface would accelerate deterioration (Leemann et al., 2010).

These observations and the results of the thermodynamic modeling agree also with the observation of Duguid et al. (2007), who observed no damage and no increase of the permeability with time in cements in contact with solutions saturated in calcium carbonate. In contrast, samples stored in the absence of calcium carbonate showed visible signs of attack and a clear increase of permeability within 3 months.

The quantified surface erosion permits assessment of the influence of the different parameters (Fig. 16). Going from a w/c of 0.50 to 0.40 has the lowest impact, while the influence of cement type and curing are in the same range. The dominating parameter is water hardness.

An extrapolation of the measured values shows that the erosion rate in the nitrification basins of the studied wastewater treatment plants is relatively low, with mean values between 0.05 mm/year (WWTP-20) and 0.20 mm/year (WWTP-32). Moreover, it has been shown that periodic cleaning substantially increases the erosion rate (Grube and Rechenberg, 1987a, 1987b; Leemann et al., 2009, 2010). Yearly erosion can be expected to be lower when the cleaning intervals are longer than the three months used in this study. When the surface of paste, mortar, or concrete is not disturbed and the leached layers remain in place, the dissolution front progresses with the square root of time (Faucon et al., 1998; Haga et al., 2005).

The planed interval for repair work in WWTPs in Switzerland is 25 years. Within this time, biodeterioration may lead to the erosion of a few millimeters of concrete within the investigated range of bicarbonate concentration. Because the reinforcement is usually covered by 30–40 mm of concrete, the durability of nitrification basins is not threatened.

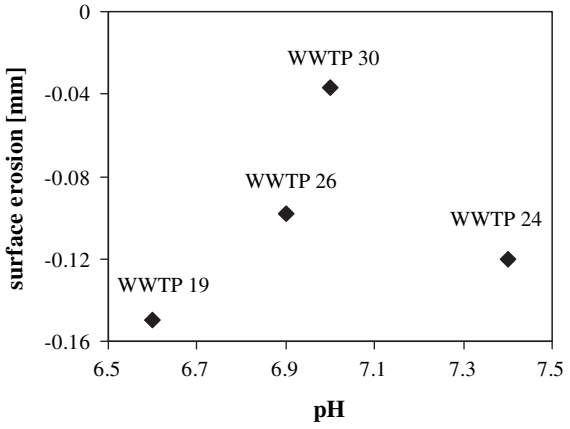

Fig. 15. Surface erosion as a function of pH in the aerated tanks.

5. Conclusions

Biodeterioration causes the erosion of the concrete surface in nitrification basins of WWTPs. Acid in the form of carbon dioxide is produced in the nitrifying biofilm and the surface of the concrete leading to the dissolution of hydration products (e.g., $Ca(OH)_2$) and the ensuing erosion. The progress of erosion is significantly influenced by the formation of different layers (layers OP, HD, and IP) below the concrete surface, increasing the distance to the unaltered concrete. In particular, the dense calcite layer HD decreases diffusivity and acts as a buffer leading to an improved resistance. Calcite is continuously dissolved at its outer side and it is continuously precipitated at its inner side, leading to an inward diffusion of the calcite layer. The removal of these layers by cleaning therefore accelerates concrete deterioration.

All studied concrete mixtures show a degree of surface erosion, but its extent depends on several parameters:

- The use of cement with a high CaO content is beneficial, as it increases the buffer capacity of the concrete.
- The density of the concrete is increased by a reduction of w/c, leading to a decreased permeability, a higher CaO content per volume and with it to an increased buffer capacity.
- Good curing optimizes cement hydration and causes a denser, less permeable microstructure. Moreover, more hydration products to neutralize protons are readily available.

However, the effect of these material parameters on concrete erosion is dominated by the influence of the biofilm layer and water characteristics in the aerated tanks of the WWTP. The high water hardness acts as a buffer, slowing down the dissolution of the concrete and the diffusion of the calcite layer into the concrete. In addition, it facilitates calcite precipitation, increasing the density of the calcite layer and with it additionally slowing down acid transport into the unaffected concrete.

The measured surface erosion rates in the nitrification basins of the studied WWTPs are only fractions of a millimeter per year and appear to present no danger to the durability of the structures within the expected lifetime of a WWTP.

Acknowledgements

Cemsuisse is acknowledged for the financial support of this project; M. Käppeli, K. Burkhard, and B. Ingold for the technical support; P. Lura for the critical review of the paper; and B. Huet for helpful discussions concerning the modeling of carbonation.

References

Aoi, Y., Miyoshi, T., Okamoto, T., Tsuneda, S., Hirata, A., Kitayama, A., Nagamune, T., 2000. Microbial ecology of nitrifying bacteria in wastewater treatment process examined by fluorescence in situ hybridization. Journal of Bioscience and Bioengineering 90, 234–240.

Bickmore, B.R., Nagy, K.L., Gray, A.K., Brinkerhoff, A.R., 2006. The effect of $Al(OH)_4^-$ on the dissolution rate of quartz. Geochimica et Cosmochimica Acta 70, 290–305.

Buenfeld, N.R., Okundi, E., 1998. Effect of cement content on transport in concrete. Magazine of Concrete Research 50, 339–351.

Davis, J.L., Nica, D., Shields, K., Roberts, D.J., 1998. Analysis of concrete from corroded sewer pipe. International Biodeterioration and Biodegradation 42, 75–84.

Dionisi, H.B., Layton, A.C., Harms, G., Gregory, I.R., Robinson, K.G., Sayler, G.S., 2002. Quantification of Nitrosomonas oligotropha-like ammonia-oxidizing bacteria and Nitrospira spp. from full-scale wastewater treatment plants by competitive PCR. Applied and Environmental Microbiology 68, 245–253.

Dove, P.M., 1994. The dissolution kinetics of quartz in sodium chloride solutions at 25 degrees to 300 degrees C. American Journal of Science 294, 665–712.

Duguid, A., Radonjic, M., Scherer, G., 2007. The effect of carbonated brine on well cement used in geologic formations. In: 12th international congress on the chemistry of cement, Montreal, Canada, TH4-10.2.

Faucon, P., Adenot, F., Jacquinot, J.F., Petit, J.C., Cabrillac, R., Jorda, M., 1998. Long-term behaviour of cement pastes used for nuclear waste disposal: Review of physico-chemical mechanisms of water degradation. Cement and Concrete Research 28, 847–857.

Grube, H., Rechenberg, W., 1987a. Betonabtrag durch chemisch angreifende saure Wässer. Beton 11, 446–451.

Grube, H., Rechenberg, W., 1987b. Betonabtrag durch chemisch angreifende saure Wässer (Fortsetzung). Beton 12, 495–498.

Gujer, W., 2010. Nitrification and me – A subjective review. Water Research 44, 1–19.

Haga, K., Sutou, S., Hironaga, M., Tanaka, M., Nagasaki, S., 2005. Effects of porosity on leaching of Ca from hardened ordinary Portland cement paste. Cement and Concrete Research 35, 1764–1775.

Hummel, W., Berner, U., Curti, E., Pearson, F.J., Thoenen, T., 2002. Nagra/PSI chemical thermodynamic data base 01/01. Universal Publishers/uPUBLISH.com, USA.

Jozsa, P.G., Stüven, R., Bock, E., Kussmaul, M., 1996. Statistical analysis of microbially influenced deterioration of concrete. DECHEMA Monographs 133, 199–208.

Juretschko, S., Timmermann, G., Schmid, M., Schleiffer, K.H., Pommerening-Röser, A., Koops, H.P., Wagner, M., 1998. Combined molecular and conventional analysis of nitrifying bacterium diversity in activated sludge: *Nitrosococcus mobilis* and Nitrospira-like bacteria as dominant populations. Applied and Environmental Microbiology 64, 3042–3051.

Kocamemi, B.A., Çeçen, F., 2009. Biodegradation of 1,2-dichloroethane (1,2-DCA) by cometabolism in a nitrifying biofilm reactor. International Biodeterioration and Biodegradation 63, 717–726.

Kulik, D., 2007. GEMS-PSI 2.2. PSI-Villigen, Switzerland. available at: http://gems.web.psi.ch/.

Lawrence, C.D.., 1984. Transport of oxygen through concrete. In: Glasser, F.P. (Ed.), The chemistry and chemically-related properties of cement. British Ceramic Society Proceedings vol. 35, 277–293.

Leemann, A., Lothenbach, B., Hoffmann, C., Bischof, S., Lunk, P., 2009. Concrete corrosion in a wastewater plant. In: Alexander, M.G., Bertron, A. (Eds.), Proceedings of the international RILEM TC 211-PAE conference on concrete in aggressive aqueous environments, performance, testing and modeling. RILEM Publications Bagneux-France, Toulouse, France, pp. 116–124.

Leemann, A., Lothenbach, B., Hoffmann, C., 2010. Biologically induced concrete deterioration in a wastewater treatment plant assessed by combining microstructural analysis with thermodynamic modeling. Cement and Concrete Research doi:10.10.16/j.cemconres.2010.03.007.

Lothenbach, B., Matschei, T., Möschner, G., Glasser, F.P., 2008. Thermodynamic modeling of the effect of temperature on the hydration and porosity of Portland cement. Cement and Concrete Research 38, 1–18.

Münch, B., Holzer, L., 2008. Contradicting geometrical concepts in pore analysis attained with electron microscopy and mercury intrusion. Journal of the American Ceramic Society 91, 4059–4067.

Neuville, N., Lecolier, E., Aouad, G., Daminot, D., 2008. Characterisation and modelling of physico-chemical degradation of cement-based materials used in oil wells. In: Schlangen, E., De Schutter, G. (Eds.), Proceedings of the international RILEM symposium on concrete modelling – CONMOD '08'. Delft, RILEM Publications, Bagneux, France, pp. 191–198.

Nica, D., Davis, J.L., Kirby, L., Zuo, G., Roberts, D.J., 2000. Isolation and characterization of microorganisms involved in the biodeterioration of concrete sewers. International Biodeterioration and Biodegradation 46, 61–68.

Okabe, S., Satoh, H., Watanbe, Y., 1999. In situ analysis of nitrifying biofilm as determined by in situ hybridization and the use of microelectrodes. Applied and Environmental Microbiology 65, 3182–3191.

Parker, C.D., 1945. The corrosion of concrete 1. Isolation of a species of bacterium associated with the corrosion of concrete exposed to atmospheres containing hydrogen sulphide. Australian Journal of Experimental Biology & Medical Science 23, 81–90.

Sand, W., 1997. Microbiological mechanisms of deterioration of inorganic substrates – A general mechanistic overview. International Biodeterioration and Biodegradation 40, 183–190.

Sand, W., Bock, E., 1991. Biodeterioration of mineral materials by microorganisms—Biogenic sulfuric and nitric acid corrosion of concrete and natural stone. Geomicrobiology Journal 9, 129–138.

Siegrist, H., Gujer, W., 1987. Demonstration of mass transfer and pH effects in a nitrifying biofilm. Water Research 21, 1481–1487.

Thoenen, T., Kulik, D., 2003. Nagra/PSI chemical thermodynamic database 01/01 for the GEM-Selektor (V.2-PSI) geochemical modeling code. PSI, Villigen. online at: http://gems.web.psi.ch/doc/pdf/TM-44-03-04-web.pdf.

Vincke, E., Boon, N., Verstraete, W., 2001. Analysis of the microbial communities on corroded concrete sewer pipes – A case study. Applied Microbiology and Biotechnology 57, 776–785.

Warscheid, Th., Braams, J., 2000. Biodeterioration of stone. International Biodeterioration and Biodegradation 46, 343–368.

You, S.J., Chen, W.Y., 2008. Ammonia oxidizing bacteria in a nitrite-accumulating membrane bioreactor. International Biodeterioration and Biodegradation 62, 244–249.